Title

Live imaging of the innate immune response in neonates reveals differential TLR2 dependent activation patterns in sterile inflammation and infection

Authors

Lalancette-Hébert, Melanie
Faustino, Joel
Thammisetty, Sai Sampath
et al.

Publication Date

2017-10-01

DOI

10.1016/j.bbi.2017.05.020

HHS Public Access

Author manuscript

Brain Behav Immun. Author manuscript; available in PMC 2018 October 01.

Published in final edited form as:

Brain Behav Immun. 2017 October ; 65: 312–327. doi:10.1016/j.bbi.2017.05.020.

Live imaging of the innate immune response in neonates reveals differential TLR2 dependent activation patterns in sterile inflammation and infection

Melanie Lalancette-Hébert[1], **Joel Faustino**[2], **Sai Sampath Thammisetty**[1], **Sophorn Chip**[2], **Zinaida S Vexler**[2,*], and **Jasna Kriz**[1,*]

[1]Department of Psychiatry and Neuroscience, Faculty of Medicine Laval University, Research Center of the IUSMQ, 2601, de la Canardière Québec (QC), G1J 2G3, CANADA

[2]Department of Neurology, University California San Francisco, San Francisco, CA 94158-0663, USA

Abstract

Activation of microglial cells in response to brain injury and/or immune stimuli is associated with a marked induction of Toll-like receptors (TLRs). While in adult brain, the contribution of individual TLRs, including TLR2, in pathophysiological cascades has been well established, their role and spatial and temporal induction patterns in immature brain are far less understood. To examine whether infectious stimuli and sterile inflammatory stimuli trigger distinct TLR2-mediated innate immune responses, we used three models in postnatal day 9 (P9) mice, a model of infection induced by systemic endotoxin injection and two models of sterile inflammation, intra-cortical IL-1β injection and transient middle cerebral artery occlusion (tMCAO). We took advantage of a transgenic mouse model bearing the dual reporter system luciferase/GFP under transcriptional control of a murine TLR2 promoter (TLR2-luc-GFP) to visualize the TLR2 response in the living neonatal brain and then determined neuroinflammation, microglial activation and leukocyte infiltration. We show that in physiological postnatal brain development the *in vivo* TLR2-luc signal undergoes a marked ~30 fold decline and temporal-spatial changes during the second and third postnatal weeks. We then show that while endotoxin robustly induces the *in vivo* TLR2-luc signal in the living brain and increases levels of several inflammatory cytokines and chemokines, the *in vivo* TLR2-luc signal is reduced after both IL-1β and tMCAO and the inflammatory response is muted. Immunofluorescence revealed that microglial cells are the predominant source of TLR2 production during postnatal brain development and in all three neonatal models studied. Flow cytometry revealed developmental changes in $CD11b^+/CD45^+$ and $CD11b^+/Ly6C^+$ cell populations, involvement of cells of the monocyte lineage, but lack of $Ly6G^+$ neutrophils or $CD3^+$ cells in acutely injured neonatal brains. Cumulatively, our results suggest

*corresponding authors: Jasna Kriz, MD, PhD, Dept. of Psychiatry and Neuroscience, Faculty of Medicine, Universite Laval, Research Centre of the IUSMQ, 2601 Chemin de la Canardière, Québec (QC), CANADA G1J 2G3, Tel +1 418 663-5000 # 6732, jasna.kriz@fmed.ulaval.ca. Zinaida Vexler, PhD, Department of Neurology, University of California San Francisco, CA 94158-0663, USA, Tel +1 415 502-2282, Zena.Vexler@ucsf.edu.

distinct TLR2 induction patterns following PAMP and DAMP - mediated inflammation in immature brain.

Keywords

Microglia; TLR2; Biophotonic/Bioluminescence Imaging; Neonate; LPS; tMCAO; IL-1β

1. Introduction

Neuroinflammation caused by infection, hypoxia-ischemia and stroke during the perinatal period contributes to increased risk for neurological and neuropsychiatric deficits and long term disabilities in children (Hagberg et al., 2015). Injury-induced inflammatory response is characterized by marked activation of the resident immune cells, microglial cells, and peripheral leukocytes, and production of inflammatory cytokines, events that may contribute to brain damage (Dirnagl et al., 1999; Iadecola and Anrather, 2011; Kriz and Lalancette-Hebert, 2009; Lo et al., 2003). Microglial cells are the principal immune cells of the brain. The current view is that once activated, microglial cells may acquire a variety of different stimulus- and context dependent immune profiles ranging from pro-inflammatory/cytotoxic to more alternative and neuroprotective phenotypes (Fernandez-Lopez et al., 2014; Pierre et al., 2017). The role of microglial cells is even more complex in immature brain, as growing evidence suggests that microglial cells play active role during brain development and early CNS homeostasis, in part by enabling neuronal synapse remodelling and phagocytosis of neurons that undergo still on-going programmed cell death in the developing brain (Paolicelli et al., 2011). Thus, inflammation and microglial activation can actively contribute to both normal physiological development and to injury in neonatal brain.

Upregulation of the pattern-recognition receptors, such as Toll-like receptors (TLRs), by activated microglial cells has been shown in injured adult brain (Akira and Takeda, 2004; Arumugam et al., 2009; Gordon, 2002; Janeway and Medzhitov, 2002; Lalancette-Hebert et al., 2009; Stridh et al., 2011; Ziegler et al., 2007) and in immature brain after H-I (Stridh et al., 2011). TLRs act via recognition of two types of ligands, the pathogen-associated molecular pattern (PAMP) ligands in response to infectious particles (Medzhitov et al., 1997) and the endogenous danger-associated molecular pattern (DAMP) ligands in response to stress or injury-derived molecules (Arumugam et al., 2009; Asea et al., 2002; Hanisch et al., 2008; Kariko et al., 2004; Matzinger, 2002). While some data suggest that immune cascades following activation of TLR receptors, like TLR2 in microglia, may have harmful effect on neonates (Du et al., 2011; Mallard et al., 2009; Mottahedin et al., 2017; Pierre et al., 2017), the role of the innate immune response in neonatal brain development and/or response to injuries remains poorly understood.

We asked if DAMP and PAMP mediated TLR2 responses lead to distinct neuroinflammatory injury patters in neonatal mice. To visualize TLR2 response in the living neonatal brain we took advantage of a transgenic mouse model bearing the dual reporter system luciferase/green fluorescent protein under transcriptional control of a murine TLR2 promoter (TLR2-luc-GFP), a reporter mouse model that we used to identify induction of TLR2 and associated

microglial activation by biophotonic/bioluminescence imaging in living adult mice subjected to stroke (Lalancette-Hebert et al., 2009; Lalancette-Hebert et al., 2012). We show that TLR2-luc signal undergoes marked ~30 fold decline and regional redistribution during the second and third postnatal weeks and that there are striking differences in the TLR2 response to endotoxin (LPS) challenge compared to sterile inflammation induced by intra-cerebral injection of IL-1β or transient middle cerebral artery occlusion (tMCAO) in postnatal day 9 (P9) mice—a robust upregulation of TLR2-luc by LPS but, surprisingly, a significant down-regulation of the TLR2-luc signal following IL-1β or tMCAO. Together with distinct LPS compared to IL-1β or tMCAO patterns of induction of inflammatory and anti-inflammatory cytokines our results strongly suggest distinct TLR2 induction patterns following PAMP and DAMP- mediated inflammation in immature brain.

2. Material and methods

2.1 Mouse model

TLR2-luc-GFP transgenic reporter mice were used to visualise TLR2 induction/microglial activation, as we described before (Lalancette-Hebert et al., 2009). Transgenic animals were identified by polymerase chain reaction (PCR) detection of the luciferase transgene with the following primers: 5′-CAG-CAG-GAT-GCT-CTC-CAG-TTC-3′ AND 5′-GGC-GCA-GTA-GGC-AAG-GTG-GT-3′. Genotyping was performed as previously described (Lalancette-Hebert et al., 2009). All experimental procedures were approved by the Laval University animal care ethics committee and are in accordance with The Guide to the Care and Use of Experimental Animals of the Canadian Council on Animal Care. All experimental procedures conducted at the University of California San Francisco were approved by the University of California San Francisco Institutional Animal Care and Use Committee and followed in accordance with the Guide for the Care and Use of Laboratory Animals (U.S. Department of Health and Human Services). Animals were given ad libitum access to food and water; housed with nesting material and shelters, and kept in rooms with temperature control and light/dark cycles.

2.2 In vivo bioluminescence/biophotonic imaging

As previously described (Cordeau et al., 2008; Lalancette-Hebert et al., 2009), bioluminescence/biophotonic images were captured using IVIS® 200 Imaging System (PerkinElmer, MA, USA). Twenty-five minutes prior to imaging session, mice received intraperitoneal (i.p.) injection of luciferase substrate D-luciferine (150 mg/kg; 20 mg/ml of D-luciferine dissolved in 0.9% saline was injected) (CaliperLS-Xenogen). 3D reconstruction of bioluminescent signal in the brain was accomplished by using diffuse luminescent imaging tomography (DLIT) algorithms (Living Image 3D Analysis Software, CaliperLS-Xenogen) (Cordeau and Kriz, 2012).

2.3 Surgical procedures

2.3.1 Stereotaxic IL-1β brain injection—P9 TLR2-luc-GFP pups of both sexes were anesthetized with 2% isoflurane in 100% oxygen at a flow rate of 1.5 l/min and placed in a stereotaxic apparatus (David Kopf Instruments). Mice received stereotaxic intracerebral injection of recombinant IL-1β (1ng) (R&D systems, MN, USA) or sterile saline solution

(0.9%) into the right parietal region of cerebral cortex. The coordinates for stereotaxic injection were the following: 2.0 mm posterior, 2.0 mm lateral (right) and –1.25 mm dorsoventral to the bregma. The injections were performed using a 33-gauge stainless steel cannula (Plastics One) connected to a 25-ml Hamilton syringe. A volume of 2 μl was infused over 2 min using a microinjection pump (model A-99; Razel Scientific Instruments). The animals were then longitudinally imaged by *in vivo* bioluminescence for a week.

2.3.2 Transient middle cerebral artery occlusion (tMCAO)—P9–P10 mice of both sexes with confirmed presence of TLR2-luc-GFP transgene were subjected to 3h tMCAO as originally described for P7 rats (Derugin et al., 2005; Derugin et al., 1998) and modified for P9–P10 mice (Woo et al., 2012). Mice were administered D-luciferine (150 mg/kg; i.p.) and were imaged 30 min later before tMCAO to obtain baseline and were imaged at 24 and 72 hrs after reperfusion. Mice were either perfusion-fixed for histology or tissue collected from injured regions and from matching contralateral regions for biochemical analysis.

2.4 LPS injection

P9 TLR2-luc-GFP pups of both sexes were injected intraperitoneally (i.p.) 1mg/kg of LPS dissolved in 0.9% sterile saline or saline. Mice were longitudinally imaged *in vivo* before and 1 and 3 days after LPS administration.

2.5 Tissue collection

For immunofluorescence analysis, anaesthetized pups were transcardially perfused with 15 ml of 0.1M PBS, followed by 4% paraformaldehyde (PFA, pH 7.4, phosphate buffered saline, PBS). Brains were postfixed overnight in 4% PFA and cryoprotected in 30% sucrose/PBS for 48 hrs, embedded into Tissue-Tek (O.C.T. compound, Sakura, USA) and frozen at −20C, cut into coronal section with a Cryostat (15-μm thick) and stored at −20C.

Pups that underwent tMCAO were deeply anesthetised with Euthasol (100 mg/kg; Virbac) and perfused transcardially with 4% PFA in 0.1M PBS (pH 7.4). Brains were post-fixed in 4% PFA overnight at 4°C, cryoprotected in 30% sucrose in 0.1 M PBS at 4°C for 48h, frozen and cut on cryostat (12 μm thick, 348 μm apart).

2.6 Immunofluorescence

Brain sections were blocked in 10% goat serum in 0.1M PBS at room temperature for 30 minutes and incubated overnight at room temperature using the following primary antibodies: mouse monoclonal anti GFP (1:750, Santa Cruz), rabbit polyclonal anti-NeuN (1:500, Cell Signaling), rat polyclonal anti CD11b (1:500, Biorad), rat anti Galectin-3 (anti-Gal-3, 1:500, American Type Culture Collection), 1:1000 rabbit anti doublecortin (DCX) (Abcam), rabbit anti-Iba1 (1:200, Wako, Japan), monoclonal anti-NeuN (1:100, Millipore), rabbit polyclonal GFAP (1:1000, DAKO) and rabbit polyclonal Ki67 (1:500, EMD Millipore). After wash in PBS, sections were incubated with appropriate Alexa-conjugated fluorescent goat secondary antiserum (ThermoFisher). Some slides were co-stained with IB4 (1:150; Life Technologies) and with DAPI. Fluorescent images were acquired either using a Zeiss LSM 700 Confocal microscope with a 10X and 20X objective using a scan zoom between 1X and 2X and analyzed with Zen software or acquired using a Zeiss Axio Imager.

Following tMCAO, a rabbit polyclonal glucose transporter 1 (Glut-1, 1:500; Millipore) was used to visualize the vessels. Some slides were co-stained with Alexa 647-conjugated *Griffonia simplicifolia* isolectin B_4 (IB4; 1:150; Life Technologies) and with DAPI. Slides were coverslipped with Prolong Gold, mounted and images captured in the penumbra and ischemic core regions in the cortex and in the corresponding contralateral regions using a Zeiss Axio Imager.Z2 microscope (Zeiss) equipped with Volocity Software (PerkinElmer).

2.7 Cytokine array analysis

Protein expression analysis of inflammatory cytokines was performed with a mouse antibody array (RaybioMouse inflammation antibody array 1.1; catalog #AAM-INF-1L; RayBiotech). Protein lysates were obtained by homogenization of brains in 500 μl of cell lysis buffer (included in the RayBiotech kit) with protease-inhibitor mixture (Complete Protease Inhibitor cocktail tablet, Roche). Protein concentration was determined for each sample and samples diluted at 300μg in 1X blocking buffer. Samples for each group (3–5 mice/group) were pooled and incubated with the array membrane overnight at 4°C. After washes, membranes were incubated with biotin-conjugated antibodies overnight at 4°C. The membranes were then processed according to RayBiotech protocol. Membranes were exposed to x-ray film (Biomax light film; #1788207; Kodak) and analyzed by ImageJ software.

2.8 Flow cytometric analysis

P6, P8 and P14 mice (n=4/age), P10 mice treated with saline or LPS at P9 (n=4/group) were transcardially perfused with ice-cold 1X DPBS to remove all blood from brain tissue. Brain samples were enzymatically (Dispase II, 2U/ml, Sigma) and mechanically dissociated and filtered through a 70 μm cell strainer to obtain a single cell suspension [Becton Dickinson (BD)]. To isolate mononuclear cell fraction, the single cell suspensions were loaded on a 30-37-70% Percoll tri-gradient (GE Healthcare) and centrifuged for 40 min at 300 × *g*. After centrifugation, mononuclear cells from the 37–70% interface were recovered and stained with appropriate antibodies. Cells were stained with anti-CD11b (PE), anti-CD45 (PerCP), anti-Ly6C (FITC), anti-Ly6G(APC-Cy7) and anti-CD3 (FITC) (BD biosciences). Samples were analyzed on a flow cytometer FACStar Plus or FACS Canto Cytometer (BD). Cells were gated using side and forward scatter to eliminate non-viable cells.

Following tMCAO, sample preparation for multi-color flow cytometry was carried out as we described (Chip et al., 2017). Briefly, mice were deeply anesthetized and transcardially perfused with 10 ml of ice-cold saline (Mg2+ and Ca2+ free Hanks Balance Salt Solution). Cortices were collected and dissociated using Neural Tissue Dissociation Kit containing papain (Miltenyi Biotec), filtered through 40 μm cell strainer, followed by myelin removal with myelin-conjugated magnetic beads (Miltenyi Biotec). The single cell suspension was passed through LS columns on a magnetic rack (Miltenyi Biotec). Using a 96-well V-bottom plate (Falcon), a density of 2×10^5 cells was plated per well. Samples were blocked for 15 min with anti-CD16/32 (Biolegend) to prevent unspecific antibody staining, followed by a single wash in FACS buffer, and then stained with the following antibodies: anti-CD11b(APC-Cy7) (Biolegend), anti-CD45(Pacific Blue) (Biolegend), anti-Ly6C(PerCP) (Biolegend), and anti-Ly6G(AF700) (Biolegend). All samples were washed once in FACS

buffer and then run on LSRII flow cytometer (BD Biosciences). BD compensation beads (BD Biosciences) were applied for compensation. Live single cells were gated and analyzed by FlowJo software (Tree Star).

2.9 Statistical analysis

All data are presented as mean ± SEM. Statistical analysis was performed by one-way ANOVA followed by post hoc comparison test (Tukey-Kramer test) or unpaired t-test. ***$p \leq 0.001$ ** $p \leq 0.01$ and *$p \leq 0.05$.

3. Results

3.1 TLR2 biophotonic/bioluminescence signal is high in the early postnatal brain and declines with brain maturation

It has been established that TLRs are the key mediators of the immune response to invading pathogens and/or of brain injury in both adult and immature brain. Growing evidence suggests that after birth, the role of the innate immune response may differ depending on the context and the stage of brain development (Hagberg et al., 2015). However, developmental patterns of TLR2 expression and the role of TLR2 signaling in injury in immature brain remain insufficiently understood. To characterize the expression patterns and the temporal dynamics of the innate immune response in early postnatal brain development, we took advantage of the TLR2-luc-GFP mice that we developed, a mouse model where TLR2 signal induction can be visualized longitudinally in the brain of living mice by biophotonic/bioluminescence imaging (Lalancette-Hebert et al., 2011; Lalancette-Hebert et al., 2009; Lalancette-Hebert et al., 2012). TLR2 biophotonic/bioluminescence imaging during postnatal brain development between P6 and P28 showed strong TLR2-luc signal in P6–P9 brain under physiological conditions (Fig. 1A–H), and decline and more compartmentalized TLR2-luc signal in specific brain regions at P14 (Fig. 1J). By P18, TLR2-luc signal intensity continued to decline and started resembling the pattern we previously observed in adult mouse (Lalancette-Hebert et al., 2009), i.e., TLR2-luc signal being predominantly restricted to the olfactory bulb region and neuroanatomical regions surrounding ventricular zone (Fig. 1K,L). Quantitative analysis of the TLR2-luc signal intensities revealed that, remarkably, early after birth, at P6–P9, TLR2 signal intensities are on average ~ 30 fold higher than the signal during early adult age; compared to that at P28, TLR2-luc signal was 33 fold higher in P6 and 27 fold higher at P9 (Fig. 1M). In addition, 2D analysis of images pointed to the presence of age-dependent regional pattern of TLR2-luc signal. To confirm that TLR-luc signal is indeed arising from the distinct brain regions in different age groups, we performed *in vivo* spectral imaging followed by DLIT analysis of the brain images (Cordeau and Kriz, 2012). As shown in Fig. 1I–L, 3D reconstruction of the TLR2-luc signal further confirmed a distinct, age-dependent neuroanatomical distribution of the TLR2-luc signal. In fact, while at P8 TLR2 expression is strong and is located in many different regions of the brain (Fig. 1I), in mature brain identifiable TLR2-luc signal becomes restricted to the olfactory bulb region, consistent with our previous observations in adult mice (Lalancette-Hebert et al., 2009). Additional analysis of the TLR2-luc signal is shown in supplemental figure 1.

We then took advantage of the dual nature of the TLR2-luc-GFP reporter mouse that co-expresses the firefly-luciferase (Luc) and green fluorescent protein (GFP) under the murine TLR2 promoter. In this model, the fluorescence signal can be used to identify the overall GFP signal, regional TLR2 expression patterns during postnatal development and the cellular origin of the signal in fixed tissue of mice that underwent *in vivo* imaging. In the cortex of P6 and P8 mice, GFP^+ cells showed ramified microglial morphology (Fig. 1N–O), and more round shaped morphology in the corpus callosum (Fig. 1R–S) and in the choroid plexus (Fig. 1V–W). At P14 and P18, very few GFP^+ cells were observed in the cortex (Fig. 1P–Q). Morphology of GFP^+ cells in the corpus callosum also changed with time to acquire an elongated shape at P14 (Fig. 1T) and star-like microglial shape at P18 (Fig. 1U). At both latter time points, GFP^+ cells were observed in the choroid plexus (Fig. 1X–Y). To better understand the dynamics and the regional expression patterns of the TLR2-luc signal in the immature brain, we next quantified GFP expression levels by optical densitometry in individual brain regions. In the cortex, GFP expression between P6–P8 remained unchanged followed by a significant decrease at P14. We observed a progressive decline of GFP expression from P6 to P18 in the corpus callosum (Fig. 1Z). In the choroid plexus, GFP expression was markedly higher than in the cortex and/or corpus callosum (Fig. 1W). These results are consistent with the regional distribution and the intensities of the TLR2-luc signal observed by live imaging. Next, to identify the cell types expressing the TLR2 driven transgene GFP we performed double-immunofluorescence analysis with cell- type specific markers, including microglial markers CD11b and Gal-3 (galectin-3), neuronal progenitor marker (DCX), neuronal marker (NeuN), astrocyte marker GFAP and endothelial cells/activated microglia marker IB4. Analysis showed that GFP^+ cells are almost exclusively $CD11b^+$ in the cortex (Fig. 2A–D) and in the corpus callosum (Fig. 2E–H). In the choroid plexus, some GFP^+ cells were $Gal\text{-}3^+$ or DCX^+ (Fig. 2I–L and supplemental Fig. 2), but there was no co-localization of the GFP^+ cells NeuN (neurons), GFAP (astrocytes) or $IB4^+$ vasculature (Fig. 2 and supplemental Fig. 2).

Considering our immunofluorescence findings that GFP^+ cells are almost exclusively $CD11b^+$, we performed flow cytometry to characterize the $CD11b^+$ population in P6–P14 brains. We gated on live single cells (Fig. 2M) and first determined the total number of $CD11b^+$ immune cells at three time points. In agreement with the previous reports (Prinz and Priller, 2014), the total number of $CD11b^+$ cells raised significantly from P6 to P14 (Fig. 2N). Subsequent gating on CD45 and CD11b revealed two distinct $CD11b^+$ populations, a $CD45^{low\text{-}med}$ population, representing resident microglial cells (Fig. 2O, top left quartile), and a $CD45^{high}$ population (Fig. 2O, top right quartile), representing activated resident microglia/macrophages, and occasional infiltrating $CD11b^+CD45^{high}$ monocytes in naïve brain. Importantly, proportion between $CD11b^+CD45^{low\text{-}med}$ and $CD11b^+CD45^{high}$ changed with brain maturation, with increased relative number of $CD11b^+CD45^{low\text{-}med}$ (Fig. 2P, left panel), and decreased relative number of $CD11b^+CD45^{high}$ cells (Fig. 2P, right panel). To further categorize $CD11b^+CD45^{high}$ population during postnatal brain development, we used Ly6C/Ly6G gating. We observed that $CD11b^+Ly6C^+Ly6G^-$ cells of the monocyte lineage, microglia and monocytes, were the predominant population, that $Ly6C^+Ly6G^-$ cells comprised <4% at P6, with further decline with brain maturation and that, and that $Ly6C^-Ly6G^+$ neutrophils comprised <1% at all ages studied (Fig. 2Q–R). Consistent with CD11b

$^{+}$ changes between P6 and P14 shown in Fig. 2P (right graph), there was significant decrease in the numbers of $Ly6C^{+}Ly6G^{-}$ and $Ly6C^{-}Ly6G^{+}$ between P6 and P14 (Fig. 2R). Taken together, our data show progressive increase in the number of $CD11b+CD45^{low/med}$ resident microglial cells between P6–P14, as well as marked decrease in intensity of the TLR2–luc and GFP signals observed both *in vivo* and in fixed brains, thus suggesting reduction in microglial activation state during brain maturation.

Taken together, bioluminescence imaging, including 3D reconstruction and analysis of cells identified by FACS, in conjunction with region-specific immunofluorescence analysis revealed the overall marked decline of the TLR2-luc signal and GFP expression and region-specific changes in localization during postnatal brain maturation. Based on expression patterns of the TLR2 driven GFP, with the exception of the choroid plexus region, in control, physiological conditions the TLR2 signal is induced/expressed in resident microglial cells.

3.2 Systemic LPS injection rapidly induces TLR2 in neonatal brain

We previously reported in the adult that systemic LPS injection induces marked TLR2 upregulation in resident microglial cells peaking 24 hrs after initial challenge (Gravel et al., 2016; Lalancette-Hebert et al., 2009). Data by others have demonstrated that LPS injection induces microglial activation in neonatal brains (Claypoole et al., 2016; Du et al., 2011). Considering that in neonatal brain TLR2 expression is already high under physiological conditions, we asked whether LPS further upregulates TLR2. Analysis of biophotonic/bioluminescence signal revealed an additional robust increase in the TLR2-luc signal following LPS challenge, with the peak at 24 hrs after injection (Fig. 3A–B and G), followed by a decline to basal level 48–72 hrs after initial stimuli (Fig. 3C–F and G). Consistent with *in vivo* imaging data, western blot analysis revealed a significant increase of both TLR2 and Iba1 protein expression 24 hrs after LPS (Fig. 3H–J).

In order to characterize a molecular signature of LPS challenge in neonatal brain we measured levels of the key inflammatory and anti-inflammatory cytokines known to be involved in control of the acute innate immune response. Cytokine array analysis 24 hrs after LPS injection demonstrated significant increase in protein expression of 10 studied pro-inflammatory cytokines as compared to saline-injected mice, including TNF-α (Fig. 3K), IL-1β (Fig. 3L), IL-17 (Fig. 3M), IL-6 (Fig. 3N), INF-γ (Fig. 3O) and MCP-1(Fig. 3T). Importantly, LPS also significantly increased the levels of several anti-inflammatory cytokines, including IL-4 (Fig. 3P) and IL-10 (Fig. 3Q), as well as growth factors M-CSF (Fig. 3R) and GM-CSF (Fig. 3S).

We next investigated cell types that upregulate TLR2 after systemic LPS challenge and whether LPS activates microglial cells in neonatal brains. Following LPS injection, double immunofluorescence analysis with cell type specific markers revealed $GFP^{+}/CD11b^{+}$ cells in the cortex (Fig. 4A–H), corpus callosum (Fig. 4J–Q) and choroid plexus (Fig. 4S–Z). Examination of microglial morphology also revealed thickening of microglial processes and acquisition of amoeboid morphology in the cortex (Fig. 4A and E) and corpus callosum (Fig. 4J and N) 24 hrs after LPS injection. Double immunofluorescence analysis revealed that GFP^{+} immunoreactivity was restricted to $CD11b^{+}$ cells and no GFP^{+} neurons and/or other cell types were found in the brains of LPS challenged neonates (supplemental Fig. 3).

Quantification of GFP immunofluorescence by optical densitometry showed significant increase of the overall GFP signal in the cortex (Fig. 4I), corpus callosum (Fig. 4R) and choroid plexus (Fig. 4AA) 24 hrs after LPS, thus, further corroborating our *in vivo* imaging results.

Inflammatory challenge such as systemic LPS injection can promote activation of resident microglial cells but can also attract immune cells from the periphery. We therefore asked if the observed robust induction of the TLR2-luc response in immature brain is associated with microglial cell activation. Although previous evidence demonstrated that in the adult brain, the systemic LPS-induced innate immune response is mediated by the resident microglia and does not lead to infiltration of the peripheral cells (Chen et al., 2012), the cellular response to LPS in immature brain is less well characterized (Cazareth et al., 2014; Pierre et al., 2016). Namely, report by Carrillo-de Savage and colleagues suggests that (Carrillo-de Sauvage et al., 2013) intraparenchymal injection of LPS may induce cell proliferation and/or infiltration of myeloid cells from the periphery. To decipher cellular components of LPS – mediated innate immune response and TLR2-luc signal induction in immature brain, we performed flow cytometry. As described above, we first gated single cells on CD45 and CD11b (see Fig. 2). Compared to vehicle injected mice (Fig. 5A, left panel, and Fig. 5B, left panel), in the LPS group, we observed a subtle but significant decrease in the number of $CD45^{low\text{-}med}$ microglial cells and a corresponding increase of the population of $CD45^{high}$ cells (Fig. 5A, right panel, and Fig. 5B, right panel). We further categorized the $CD11b^{+}CD45^{high}$ population by gating on Ly6C/Ly6G as we described in Fig. 2C. LPS injection significantly increased the $Ly6C^{-}/Ly6G^{-}$ cell population by 1% and $Ly6C^{+}/Ly6G^{-}$ cell population by 3.2%. Percent of neutrophils (Fig. 5D right panel) or CD3+ lymphocytes (Fig. 5E–F) remained small (<1%) and was not affected by LPS injection. We next asked whether LPS-induced increase in TLR2-GFP signal can be caused by the proliferation of microglial cells. Triple immunofluorescence analysis for proliferation marker Ki67 in combination with GFP and CD11b showed very few triple $GFP^{+}CD11b^{+}Ki67^{+}$ cells in the cortex (Fig. 5G–I and P–R) or in the corpus callosum (Fig. 5J–L and S–U) in P10 CTL or 24 hrs after LPS, but few $GFP^{+}CD11b^{+}Ki67^{+}$ cells in the choroid plexus, thus suggesting that systemic LPS injection may induce a limited proliferation of a subset of cells in choroid plexus region (Fig. 5M–O and V–X). Taken together, our results suggest that robust induction of the TLR2-luc signal observed following systemic LPS challenge in P9–P10 mice, as in adult brain, is caused predominantly by a marked activation of resident microglial cells (Chen et al., 2012).

3.3 Brain response following IL-1β injection and focal arterial stroke in neonates is characterized by downregulation of the innate immune response

Recent studies suggest that TLR2 may have age-dependent role in the brain response to injury and associated DAMPS (Eklind et al., 2004; Mallard et al., 2009). Therefore, we analyzed the TLR2 signal patterns in living brains in two different models of brain injury in neonatal mice, following intra-cortical IL-1β injection or tMCAO.

3.3.1 Intracortical IL-1β injection mutes the inflammatory response and does not induce TLR2—Previous evidence of the inflammatory response by intracortical IL-1β

injection in pups yielded conflicting results (Cai et al., 2004; Wang et al., 2011). Some studies suggested that IL-1β does not induce strong microglial activation (Cai et al., 2004), while others reported a role of IL-1β injection in inflammation in chronic pain and/or neuronal death (Wang et al., 2011). We reported increased IL-1β in the blood and then in injured brain regions in a neonatal rat stroke model (Denker et al., 2007), but lesser magnitude of effects in a neonatal mouse stroke model (Woo et al., 2012). We imaged P9 TLR2-luc-GFP mice following IL-1β injection or vehicle and observed a significant decrease of the TLR2-luc signal compared to that in saline injected mice at 24 hours (Fig. 6A–B, G). A further significant decrease of the TLR2-luc signal was observed 2 days after injection in both saline or IL-1β treated mice (Fig. 6G), consistent with developmental decline in the TLR2 signal (Fig 1). The observed decrease in the TLR2-luc signal *in vivo* was further confirmed by western blot analysis (Fig. 6H), In fact, consistent with *in vivo* imaging data, quantification of TLR2 and Iba1 protein levels revealed a significant decrease 24 hrs after IL-1β injection (Fig. 6I–J). In keeping with the observed decrease in the TLR2-luc signal, compared to saline treated mice, the levels of several studied cytokines were significantly lower in the brains of IL-1β injected mice, Quantitative cytokine array analysis revealed a significant decrease in the levels of IL1β, Il–17, IL-6, IFNγ and GM-SCF. The levels of TNF-α, IL-4 and M-CSF remained unchanged (Fig. 6K–T).

Interestingly, double immunofluorescence showed distinct cell type specific distribution of the TLR2-GFP signal adjacent to and distant from the injection site 24 hrs after injection. While adjacent to the injection site, in saline (Fig. 6U–X) and IL-1β injected mice (Fig. 6Y–BB) GFP^+ cells were $NeuN^+$ neurons, $CD11b^+$ microglia/macrophages were the principal cell type upregulating TLR2 distant from the injection site. Neurons expressed GFP+ adjacent to the injection site, likely as a response to stress and/or inflicted injury at injection site.

Altogether, *in vivo* TLR2 imaging analysis, western blot analysis as well as cytokine array analysis consistently showed decrease in the markers of inflammatory response following sterile stimuli, thus suggesting distinct mechanisms of the immature brain responses to cope with non-infectious injury and/or stress. Furthermore, our results showed that microglial cells do not activate innate immune response cascade within 24 hrs after intracortical IL-1β injection.

3.3.2 Lack of acute TLR2 induction in neonatal TLR2-luc-GFP mice after acute tMCAO—Given markedly different innate immune responses following LPS challenge and in a sterile brain injury induced by IL-1β injection, we asked if tMCAO in P9–P10 mice, another type of sterile injury, affects the innate response. Our previous studies in neonatal rat and mouse stroke tMCAO models have shown that microglial cells contribute to endogenous protection, at least during acute and subchronic injury phases (Faustino et al., 2011; Fernandez-Lopez et al., 2016), and that mRNA levels for several TLRs remain mostly unchanged in ischemic-reperfused brain regions as well as in microglial cells acutely dissociated from neonatal brain 24 hrs after tMCAO (Li et al., 2015). In this study we determined TLR2-luc signal after tMCAO directly in the living neonatal TLR2-luc-GFP brain (Fig. 7A–E). Quantification of the TLR2-luc signal in the entire brain 24 hrs after reperfusion showed the overall significant reduction of TLR2-luc signal (Fig. 7B and D) and

restoration of the signal by 72 hrs. Compared to contralateral hemisphere, TLR2-luc signal was significantly higher in most injured mice but not in all mice (Fig. 7C and E). Measurements of injury in Nissl-stained brains confirmed consistent injury in all imaged mice, with injury volume occupying 34.5 ± 3.5% of ipsilateral hemisphere (n=7). In addition, we used the presence of a characteristic pattern of spectrin cleavage by calpain-dependent mechanism (150kDa, Fig. 7F) or by caspase-3 mechanism (120kDa, Fig. 7F) to confirm successful occlusion of the MCA in mice designated for biochemical measurements, method that we extensively used in the past (Chip et al., 2017; Fernandez-Lopez et al., 2016; Li et al., 2015; Woo et al., 2012). Unilateral TLR2 upregulation was observed in injured regions at 72 hrs but not at 24 hrs after tMCAO (Fig. 7C and E), consistent with *in vivo* imaging results (Fig. 7A–C).

Analysis of cellular origin of the TLR2 driven GFP transgene by double immunofluorescence revealed that essentially all GFP^+ cells were $IB4^+$ activated microglial cells in the ischemic core and penumbra (Fig. 7G–N) and that only a small fraction of GFP^+ cells were GFP^+NeuN^+ cells (Fig. 7G–N), again showing that microglia/macrophages are the predominant cell type expressing TLR2 under sterile inflammation. Consistent with *in vivo* TLR2-luc data, the strongest TLR2-GFP signal was observed in the choroid plexus (Fig. 7O–Q).

Multiple cytokine array analysis 24 hrs after tMCAO showed significantly decreased levels of major pro-inflammatory cytokine in injured compared to matching contralateral regions, including TNF-α (Fig. 8A), IL-1β (Fig. 8B), IL-17 (Fig. 8C) and INFγ (Fig. 8E). On the opposite, the level of IL-6 (Fig. 8D) and MCP-1 (Fig. 8J) were significantly increased in injured regions. Protein levels of anti-inflammatory cytokines IL-4 and IL-10 and growth factors M-CSF and MGM-CSF were not significantly changed compared to those in matching contralateral regions (Fig. 8).

We then asked if injury was associated with infiltration of monocytes and neutrophils. Using a strategy described in Fig. 2M–O, we gated on single cells from whole tissue lysates (Fig. 8K) and used unstained negative control (Fig. 8L) to identify $CD11b^+CD45^+$ population in contralateral (Fig. 8M) and injured (Fig. 8O) regions. As we previously reported, there was a shift in signal intensity and accumulation of $CD11b^+CD45^+$ cells (Fig. 8M–O)(Chip et al., 2017; Li et al., 2015). There was only a small (<1%) $CD11b^+CD45^+Ly6G^+$ subpopulation in both contralateral (Fig. 8N) and injured (Fig. 8P) regions, indicating minimal neutrophil infiltration after tMCAO.

4. Discussion

The innate immune response is a fundamental mechanism involved in the regulation of brain inflammation caused by sterile inflammation or by infection, but the relative role of individual TLRs under sterile and infectious stimuli is less well characterized. In this study, we report that TLR2 is highly expressed in early postnatal brain, between P6–P9, that TLR2 expression rapidly decreases with postnatal brain maturation under physiological conditions and becomes restricted to the olfactory bulb at P28. Importantly, flow cytometry revealed that the observed *in vivo* TLR2-luc signal indeed originates from activated resident brain

microglia/macrophages. We then show that bacterial inflammation caused by systemic LPS injection induces TLR2 in microglial cells and promotes synthesis and/or secretion of inflammatory mediators, whereas sterile inflammation, induced by either intra-cortical IL-1β injection or tMCAO, downregulates the innate immune response, limits TLR2 induction and blunts production of inflammatory cytokines. While microglial cells are the predominant cell type that expresses TLR2 in all injury models studied, our findings indicate a scenario-specific adaptable role of the innate immune response as a reaction to injury or infection in neonates.

The inflammatory response is a defense reaction against divers insults designed to remove noxious agents and to limit their detrimental effects. TLRs are active responders to and mediators of infection as well as sterile inflammation and brain injury in stroke. While TLR4 seems to be purely injurious in both experimental stroke (Kilic et al., 2008; Lehnardt et al., 2007; Saito et al., 2000) and human stroke (Beschorner et al., 2002), the role of TLR2 is more complex. Namely, it appears that TLR2 may elicit context- and tissue-dependent effects that are either injurious (Abe et al., 2010; Ziegler et al., 2007) or beneficial (Hua et al., 2009; Rolls et al., 2007) based on the type(s) of heterodimers that it forms with TLR1 and TLR4 (Abe et al., 2010). While TLR downstream signaling pathways are relatively well described, the mechanisms facilitating ligand recognition by TLRs remain poorly understood. While we and others have shown that timely TLR2 induction is needed after brain injury to limit evolution of brain damage in the adult (Bohacek et al., 2012; Lalancette-Hebert et al., 2007), the role of inflammation and innate immunity is more complex in injured immature brain. For example, in the developing brain, the role of TLR receptors is context-dependent—bacterial Vs. sterile— and age-dependent—term brain Vs. preterm brain (Mallard et al., 2009). In the hypoxia-ischemia model at term, neither TLR2 agonist (Eklind et al., 2004) nor genetic deletion of TLR2's downstream affecter, MyD88 (Mallard et al., 2009), affect injury, whereas genetic TLR2 deletion decreases infarct volume (Stridh et al., 2011). At the same time, systemic LPS-induced TLR4 stimulation and TLR2 stimulation by its ligand Pam3CSK4 during P3–P11 produce differing responses at P12 (Du et al., 2011). Pam3CSK4-induced TLR2 activation in P9 mice exerts robust leukocyte trafficking via the choroid plexus (Mottahedin et al., 2017). Interestingly, Pam3CSK4 but not LPS induces IL-1β when stimulation occurs in the premature brain (Stridh et al., 2011). While IL-1β is generally considered injurious, genetic manipulations of the pathway showed rather complex effects on hypoxia-ischemia injury in neonatal brain (Doverhag et al., 2010; Girard et al., 2008; Savard et al., 2015; Stridh et al., 2011). TLR2 is regulated in hypoxia-ischemia and by LPS (Triantafilou and Triantafilou, 2002), counteracting the proliferation of neuronal progenitor cells and leading to defects in brain plasticity and behaviour (Yuan et al., 2010).

Considering that it is becoming increasingly clear that innate immune system activation can modulate postnatal brain development (Bsibsi et al., 2002; Jack et al., 2005; Yuan et al., 2010) and that timely modulation of innate immunity is instrumental in the early brain homeostasis and brain development, we investigated *in vivo* TLR2 expression in normally developing brain and in injured neonatal brain in the context of systemic bacterial challenge and in two models of sterile brain injury. Our results revealed a markedly higher TLR2 expression in multiple brain regions, most prominently in the choroid plexus and in the

corpus callosum in early postnatal period, that declines by P28. As in adult brain (Andreasson et al., 2016; Grabert et al., 2016; Lawson et al., 1990; Olah et al., 2011), we also observed a broad range of microglial morphologies in immature brain. We demonstrate that GFP^+ cells are mainly resident microglia/macrophages during physiological brain development and that while microglial cells have a more “activated-like” amoeboid round shape morphology at P6, they undergo ramification by P14, in parallel with a decrease in the $CD11b^+/CD45^{high}$ cell population. As suggested by others, this may be in part related to a decline in neuronal programmed cell death and reduced pruning by P14 (Ikonomidou et al., 1999) (Paolicelli et al., 2011). Importantly, upon both types of injury, resident microglia/macrophages remain the principal cell type expressing TLR2, with only a few $NeuN^+$ cells within injured regions.

The detrimental effects of microglial activation has been linked to induction of pattern recognition receptors, TLRs, implicated in response to danger signals in the brain. Viral or bacterial infections are associated with significant lifelong deficits and mortality (Muller, 2016). For example, 40% of newborns who survive herpes, encephalitis or sepsis develop neurologic impairments (Mwaniki et al., 2012). LPS has been shown to induce microglial activation, TLR2 expression in the CNS and production of pro-inflammatory cytokines like IL-1β and IL-6 (Laflamme et al., 2001; Monje et al., 2003; Strunk et al., 2014; Turrin et al., 2001; Vallieres and Rivest, 1997). Consistent with this notion, we observed a strong transient increase in TLR2-luc signal 24 hrs after LPS administration, which was accompanied by an increase in several major inflammatory cytokines, but anti-inflammatory cytokines as well. The increase in cytokine production can probably be attributed to resident glial cells since it has been shown that, although LPS can cause the release of CCl5 and MCP-1 in the brain, it does not promote a significant leukocyte infiltration into brain parenchyma, at least not early (Mottahedin et al., 2017). Change in morphology of GFP^+ microglial cells toward a more activated morphological phenotype, accumulation of $CD45^{high}/Ly6C^+$ cells and the negligible number of $Ly6G^+$ and $CD3^+$ cells that we observe are in agreement with data by others and suggest a major role for cells of the monocyte lineage in response to LPS.

Previous studies have shown that TLR expression can be regulated in a stimulus-dependant and cell-type specific manner (Iwasaki and Medzhitov, 2004; Muzio et al., 2000; Visintin et al., 2001; Yoon et al., 2008). IL-1β administration is often used as a model of apoptotic cell death despite controversial reports (Allan, 2002; Cai et al., 2004; Holmin and Mathiesen, 2000; Iwasaki and Medzhitov, 2004; Loddick and Rothwell, 1996; Muzio et al., 2000; Patel et al., 2003; Visintin et al., 2001; Yoon et al., 2008). Here, we show that at 24 hrs neither IL-1β injection nor tMCAO increase TLR2 expression and/or induce marked inflammatory cytokine production. These data are consistent with our earlier observations that microglial cells are intrinsically protective after neonatal stroke (Faustino et al., 2011; Fernandez-Lopez et al., 2014) and that injury is not associated with increased TLR2/3/4 gene induction 24–72 hrs after neonatal stroke (Li et al., 2015). Considering that cytokines produced in microglia vs. monocytes can exert distinct or even opposite effects in stroke (Lambertsen et al., 2009), it would be important to understand the relative contribution of microglial cells Vs. monocytes into injury. This important question continues to be unresolved because microglia and monocytes share a vast majority of antigens and antibodies to antigens specific to either

microglia or monocytes are not commercially available. While we share the same limitations, we demonstrate the predominant presence of $CD11b^{+}/CD45^{+}/Ly6C^{low}$ cells in naïve brains and in brains following IL-1β injection or tMCAO, a population comprised of activated microglial and beneficial monocytes.

Our findings show that in distinct kinds of injury to neonatal brain—infectious or sterile—the cytokine response is vastly different, but that the main TLR2 expressing cell type are microglial cells. These observations raise a fundamental question about whether similar or distinct signal transduction repertoires in microglial cells are involved under the studied conditions. Given the presence of an array of inducible molecules in microglia in the adult (Lucin and Wyss-Coray, 2009) and that both brain immaturity and microglial cell immaturity greatly affect the function of microglial cells (Butovsky et al., 2014; Hagberg et al., 2015), it is likely that an interplay between many pathways exert the differential response.

In conclusion, we show for the first time that TLR2 expression is age-dependent under both physiological conditions as well as after injury, that the involvement of TLR2 in stroke in the adult and in the neonate is vastly different, and that the underlying “signatures” of the TLR2 response to sterile and non-sterile inflammation are vastly different. This study raises many questions important for translational research, because the improved understanding of TLR2-mediated microglia-mediated responses to infection or injury would allow for identification of new pharmacological targets. Furthermore, the enhanced understanding of how to use TLR signalling to precondition the susceptible neonates or neonates who are at higher risk for stroke or hypoxia-ischemia due to infection in utero, would allow us to minimize long-term consequences of injury during the neonatal period.

Supplementary Material

Refer to Web version on PubMed Central for supplementary material.

Acknowledgments

The authors acknowledge Genevieve Soucy for technical help. The work was supported by RO1 NS44025 (Z.S.V& J.K.), RO1 NS76726 (Z.S.V. & J.K.), R21 NS098514 ((Z.S.V.).

References

Abe Y, Kawakami A, Osaka M, Uematsu S, Akira S, Shimokado K, Sacks FM, Yoshida M. Apolipoprotein CIII induces monocyte chemoattractant protein-1 and interleukin 6 expression via Toll-like receptor 2 pathway in mouse adipocytes. Arterioscler Thromb Vasc Biol. 2010; 30:2242–2248. [PubMed: 20829510]

Akira S, Takeda K. Toll-like receptor signalling. Nature reviews Immunology. 2004; 4:499–511.

Allan SM. Varied actions of proinflammatory cytokines on excitotoxic cell death in the rat central nervous system. J Neurosci Res. 2002; 67:428–434. [PubMed: 11835309]

Andreasson KI, Bachstetter AD, Colonna M, Ginhoux F, Holmes C, Lamb B, Landreth G, Lee DC, Low D, Lynch MA, Monsonego A, O’Banion MK, Pekny M, Puschmann T, Russek-Blum N, Sandusky LA, Selenica ML, Takata K, Teeling J, Town T, Van Eldik LJ. Targeting innate immunity for neurodegenerative disorders of the central nervous system. Journal of neurochemistry. 2016; 138:653–693. [PubMed: 27248001]

Arumugam TV, Okun E, Tang SC, Thundyil J, Taylor SM, Woodruff TM. Toll-like receptors in ischemia-reperfusion injury. Shock. 2009; 32:4–16. [PubMed: 19008778]

Asea A, Rehli M, Kabingu E, Boch JA, Bare O, Auron PE, Stevenson MA, Calderwood SK. Novel signal transduction pathway utilized by extracellular HSP70: role of toll-like receptor (TLR) 2 and TLR4. The Journal of biological chemistry. 2002; 277:15028–15034. [PubMed: 11836257]

Beschorner R, Schluesener HJ, Gozalan F, Meyermann R, Schwab JM. Infiltrating CD14+ monocytes and expression of CD14 by activated parenchymal microglia/macrophages contribute to the pool of CD14+ cells in ischemic brain lesions. Journal of neuroimmunology. 2002; 126:107–115. [PubMed: 12020962]

Bohacek I, Cordeau P, Lalancette-Hebert M, Gorup D, Weng YC, Gajovic S, Kriz J. Toll-like receptor 2 deficiency leads to delayed exacerbation of ischemic injury. Journal of neuroinflammation. 2012; 9:191. [PubMed: 22873409]

Bsibsi M, Ravid R, Gveric D, van Noort JM. Broad expression of Toll-like receptors in the human central nervous system. J Neuropathol Exp Neurol. 2002; 61:1013–1021. [PubMed: 12430718]

Butovsky O, Jedrychowski MP, Moore CS, Cialic R, Lanser AJ, Gabriely G, Koeglsperger T, Dake B, Wu PM, Doykan CE, Fanek Z, Liu L, Chen Z, Rothstein JD, Ransohoff RM, Gygi SP, Antel JP, Weiner HL. Identification of a unique TGF-beta-dependent molecular and functional signature in microglia. Nature neuroscience. 2014; 17:131–143. [PubMed: 24316888]

Cai Z, Lin S, Pang Y, Rhodes PG. Brain injury induced by intracerebral injection of interleukin-1beta and tumor necrosis factor-alpha in the neonatal rat. Pediatric research. 2004; 56:377–384. [PubMed: 15201401]

Carrillo-de Sauvage MA, Maatouk L, Arnoux I, Pasco M, Sanz Diez A, Delahaye M, Herrero MT, Newman TA, Calvo CF, Audinat E, Tronche F, Vyas S. Potent and multiple regulatory actions of microglial glucocorticoid receptors during CNS inflammation. Cell Death Differ. 2013; 20:1546–1557. [PubMed: 24013726]

Cazareth J, Guyon A, Heurteaux C, Chabry J, Petit-Paitel A. Molecular and cellular neuroinflammatory status of mouse brain after systemic lipopolysaccharide challenge: importance of CCR2/CCL2 signaling. Journal of neuroinflammation. 2014; 11:132. [PubMed: 25065370]

Chen Z, Jalabi W, Shpargel KB, Farabaugh KT, Dutta R, Yin X, Kidd GJ, Bergmann CC, Stohlman SA, Trapp BD. Lipopolysaccharide-induced microglial activation and neuroprotection against experimental brain injury is independent of hematogenous TLR4. J Neurosci. 2012; 32:11706–11715. [PubMed: 22915113]

Chip S, Fernandez-Lopez D, Li F, Faustino J, Derugin N, Vexler ZS. Genetic deletion of galectin-3 enhances neuroinflammation, affects microglial activation and contributes to sub-chronic injury in experimental neonatal focal stroke. Brain, behavior, and immunity. 2017; 60:270–281.

Claypoole LD, Zimmerberg B, Williamson LL. Neonatal lipopolysaccharide treatment alters hippocampal neuroinflammation, microglia morphology and anxiety-like behavior in rats selectively bred for an infantile trait. Brain, behavior, and immunity. 2016

Cordeau P Jr, Lalancette-Hebert M, Weng YC, Kriz J. Live imaging of neuroinflammation reveals sex and estrogen effects on astrocyte response to ischemic injury. Stroke; a journal of cerebral circulation. 2008; 39:935–942.

Cordeau P, Kriz J. Real-time imaging after cerebral ischemia: model systems for visualization of inflammation and neuronal repair. Methods in enzymology. 2012; 506:117–133. [PubMed: 22341222]

Denker SP, Ji S, Dingman A, Lee SY, Derugin N, Wendland MF, Vexler ZS. Macrophages are comprised of resident brain microglia not infiltrating peripheral monocytes acutely after neonatal stroke. Journal of neurochemistry. 2007; 100:893–904. [PubMed: 17212701]

Derugin N, Dingman A, Wendland MF, Fox C, Bollen A, Vexler ZS. Magnetic resonance imaging as a surrogate measure for histological sub-chronic endpoint in a neonatal rat stroke model. Brain research. 2005; 1066:49–56. [PubMed: 16336947]

Derugin N, Ferriero DM, Vexler ZS. Neonatal reversible focal cerebral ischemia: a new model. Neurosci Res. 1998; 32:349–353. [PubMed: 9950062]

Dirnagl U, Iadecola C, Moskowitz MA. Pathobiology of ischaemic stroke: an integrated view. Trends in neurosciences. 1999; 22:391–397. [PubMed: 10441299]

Doverhag C, Hedtjarn M, Poirier F, Mallard C, Hagberg H, Karlsson A, Savman K. Galectin-3 contributes to neonatal hypoxic-ischemic brain injury. Neurobiology of disease. 2010; 38:36–46. [PubMed: 20053377]

Du X, Fleiss B, Li H, D'Angelo B, Sun Y, Zhu C, Hagberg H, Levy O, Mallard C, Wang X. Systemic stimulation of TLR2 impairs neonatal mouse brain development. PloS one. 2011; 6:e19583. [PubMed: 21573120]

Eklind S, Arvidsson P, Hagberg H, Mallard C. The role of glucose in brain injury following the combination of lipopolysaccharide or lipoteichoic acid and hypoxia-ischemia in neonatal rats. Dev Neurosci. 2004; 26:61–67. [PubMed: 15509900]

Faustino JV, Wang X, Johnson CE, Klibanov A, Derugin N, Wendland MF, Vexler ZS. Microglial cells contribute to endogenous brain defenses after acute neonatal focal stroke. J Neurosci. 2011; 31:12992–13001. [PubMed: 21900578]

Fernandez-Lopez D, Faustino J, Klibanov AL, Derugin N, Blanchard E, Simon F, Leib SL, Vexler ZS. Microglial Cells Prevent Hemorrhage in Neonatal Focal Arterial Stroke. J Neurosci. 2016; 36:2881–2893. [PubMed: 26961944]

Fernandez-Lopez D, Natarajan N, Ashwal S, Vexler ZS. Mechanisms of perinatal arterial ischemic stroke. J Cereb Blood Flow Metab. 2014; 34:921–932. [PubMed: 24667913]

Girard S, Kadhim H, Larouche A, Roy M, Gobeil F, Sebire G. Pro-inflammatory disequilibrium of the IL-1 beta/IL-1ra ratio in an experimental model of perinatal brain damages induced by lipopolysaccharide and hypoxia-ischemia. Cytokine. 2008; 43:54–62. [PubMed: 18511291]

Gordon S. Pattern recognition receptors: doubling up for the innate immune response. Cell. 2002; 111:927–930. [PubMed: 12507420]

Grabert K, Michoel T, Karavolos MH, Clohisey S, Baillie JK, Stevens MP, Freeman TC, Summers KM, McColl BW. Microglial brain region-dependent diversity and selective regional sensitivities to aging. Nature neuroscience. 2016; 19:504–516. [PubMed: 26780511]

Gravel M, Beland LC, Soucy G, Abdelhamid E, Rahimian R, Gravel C, Kriz J. IL-10 Controls Early Microglial Phenotypes and Disease Onset in ALS Caused by Misfolded Superoxide Dismutase 1. J Neurosci. 2016; 36:1031–1048. [PubMed: 26791230]

Hagberg H, Mallard C, Ferriero DM, Vannucci SJ, Levison SW, Vexler ZS, Gressens P. The role of inflammation in perinatal brain injury. Nat Rev Neurol. 2015; 11:192–208. [PubMed: 25686754]

Hanisch UK, Johnson TV, Kipnis J. Toll-like receptors: roles in neuroprotection? Trends in neurosciences. 2008; 31:176–182. [PubMed: 18329736]

Holmin S, Mathiesen T. Intracerebral administration of interleukin-1beta and induction of inflammation, apoptosis, and vasogenic edema. J Neurosurg. 2000; 92:108–120. [PubMed: 10616089]

Hua F, Ma J, Ha T, Kelley JL, Kao RL, Schweitzer JB, Kalbfleisch JH, Williams DL, Li C. Differential roles of TLR2 and TLR4 in acute focal cerebral ischemia/reperfusion injury in mice. Brain research. 2009; 1262:100–108. [PubMed: 19401158]

Iadecola C, Anrather J. Stroke research at a crossroad: asking the brain for directions. Nature neuroscience. 2011; 14:1363–1368. [PubMed: 22030546]

Ikonomidou C, Bosch F, Miksa M, Bittigau P, Vockler J, Dikranian K, Tenkova TI, Stefovska V, Turski L, Olney JW. Blockade of NMDA receptors and apoptotic neurodegeneration in the developing brain. Science. 1999; 283:70–74. [PubMed: 9872743]

Iwasaki A, Medzhitov R. Toll-like receptor control of the adaptive immune responses. Nat Immunol. 2004; 5:987–995. [PubMed: 15454922]

Jack CS, Arbour N, Manusow J, Montgrain V, Blain M, McCrea E, Shapiro A, Antel JP. TLR signaling tailors innate immune responses in human microglia and astrocytes. J Immunol. 2005; 175:4320–4330. [PubMed: 16177072]

Janeway CA Jr, Medzhitov R. Innate immune recognition. Annual review of immunology. 2002; 20:197–216.

Kariko K, Weissman D, Welsh FA. Inhibition of toll-like receptor and cytokine signaling--a unifying theme in ischemic tolerance. J Cereb Blood Flow Metab. 2004; 24:1288–1304. [PubMed: 15545925]

Kilic U, Kilic E, Matter CM, Bassetti CL, Hermann DM. TLR-4 deficiency protects against focal cerebral ischemia and axotomy-induced neurodegeneration. Neurobiology of disease. 2008; 31:33–40. [PubMed: 18486483]

Kriz J, Lalancette-Hebert M. Inflammation, plasticity and real-time imaging after cerebral ischemia. Acta neuropathologica. 2009; 117:497–509. [PubMed: 19225790]

Laflamme N, Soucy G, Rivest S. Circulating cell wall components derived from gram-negative, not gram-positive, bacteria cause a profound induction of the gene-encoding Toll-like receptor 2 in the CNS. Journal of neurochemistry. 2001; 79:648–657. [PubMed: 11701768]

Lalancette-Hebert M, Gowing G, Simard A, Weng YC, Kriz J. Selective ablation of proliferating microglial cells exacerbates ischemic injury in the brain. J Neurosci. 2007; 27:2596–2605. [PubMed: 17344397]

Lalancette-Hebert M, Julien C, Cordeau P, Bohacek I, Weng YC, Calon F, Kriz J. Accumulation of dietary docosahexaenoic acid in the brain attenuates acute immune response and development of postischemic neuronal damage. Stroke; a journal of cerebral circulation. 2011; 42:2903–2909.

Lalancette-Hebert M, Phaneuf D, Soucy G, Weng YC, Kriz J. Live imaging of Toll-like receptor 2 response in cerebral ischaemia reveals a role of olfactory bulb microglia as modulators of inflammation. Brain. 2009; 132:940–954. [PubMed: 19153151]

Lalancette-Hebert M, Swarup V, Beaulieu JM, Bohacek I, Abdelhamid E, Weng YC, Sato S, Kriz J. Galectin-3 is required for resident microglia activation and proliferation in response to ischemic injury. J Neurosci. 2012; 32:10383–10395. [PubMed: 22836271]

Lambertsen KL, Clausen BH, Babcock AA, Gregersen R, Fenger C, Nielsen HH, Haugaard LS, Wirenfeldt M, Nielsen M, Dagnaes-Hansen F, Bluethmann H, Faergeman NJ, Meldgaard M, Deierborg T, Finsen B. Microglia protect neurons against ischemia by synthesis of tumor necrosis factor. J Neurosci. 2009; 29:1319–1330. [PubMed: 19193879]

Lawson LJ, Perry VH, Dri P, Gordon S. Heterogeneity in the distribution and morphology of microglia in the normal adult mouse brain. Neuroscience. 1990; 39:151–170. [PubMed: 2089275]

Lehnardt S, Lehmann S, Kaul D, Tschimmel K, Hoffmann O, Cho S, Krueger C, Nitsch R, Meisel A, Weber JR. Toll-like receptor 2 mediates CNS injury in focal cerebral ischemia. Journal of neuroimmunology. 2007; 190:28–33. [PubMed: 17854911]

Li F, Faustino J, Woo MS, Derugin N, Vexler ZS. Lack of the scavenger receptor CD36 alters microglial phenotypes after neonatal stroke. Journal of neurochemistry. 2015; 135:445–452. [PubMed: 26223273]

Lo EH, Dalkara T, Moskowitz MA. Mechanisms, challenges and opportunities in stroke. Nature reviews. 2003; 4:399–415.

Loddick SA, Rothwell NJ. Neuroprotective effects of human recombinant interleukin-1 receptor antagonist in focal cerebral ischaemia in the rat. J Cereb Blood Flow Metab. 1996; 16:932–940. [PubMed: 8784237]

Lucin KM, Wyss-Coray T. Immune activation in brain aging and neurodegeneration: too much or too little? Neuron. 2009; 64:110–122. [PubMed: 19840553]

Mallard C, Wang X, Hagberg H. The role of Toll-like receptors in perinatal brain injury. Clin Perinatol. 2009; 36:763–772. v–vi. [PubMed: 19944834]

Matzinger P. An innate sense of danger. Annals of the New York Academy of Sciences. 2002; 961:341–342. [PubMed: 12081934]

Medzhitov R, Preston-Hurlburt P, Janeway CA Jr. A human homologue of the Drosophila Toll protein signals activation of adaptive immunity. Nature. 1997; 388:394–397. [PubMed: 9237759]

Monje ML, Toda H, Palmer TD. Inflammatory blockade restores adult hippocampal neurogenesis. Science. 2003; 302:1760–1765. [PubMed: 14615545]

Mottahedin A, Svedin P, Nair S, Mohn CJ, Wang X, Hagberg H, Ek J, Mallard C. Systemic activation of Toll-like receptor 2 suppresses mitochondrial respiration and exacerbates hypoxic-ischemic injury in the developing brain. J Cereb Blood Flow Metab. 2017; 37:1192–1198. [PubMed: 28139935]

Muller WJ. 2016Treatment of perinatal viral infections to improve neurologic outcomes. Pediatric research.

Muzio M, Bosisio D, Polentarutti N, D'Amico G, Stoppacciaro A, Mancinelli R, van't Veer C, Penton-Rol G, Ruco LP, Allavena P, Mantovani A. Differential expression and regulation of toll-like receptors (TLR) in human leukocytes: selective expression of TLR3 in dendritic cells. J Immunol. 2000; 164:5998–6004. [PubMed: 10820283]

Mwaniki MK, Atieno M, Lawn JE, Newton CR. Long-term neurodevelopmental outcomes after intrauterine and neonatal insults: a systematic review. Lancet. 2012; 379:445–452. [PubMed: 22244654]

Olah M, Biber K, Vinet J, Boddeke HW. Microglia phenotype diversity. CNS Neurol Disord Drug Targets. 2011; 10:108–118. [PubMed: 21143141]

Paolicelli RC, Bolasco G, Pagani F, Maggi L, Scianni M, Panzanelli P, Giustetto M, Ferreira TA, Guiducci E, Dumas L, Ragozzino D, Gross CT. Synaptic pruning by microglia is necessary for normal brain development. Science. 2011; 333:1456–1458. [PubMed: 21778362]

Patel HC, Boutin H, Allan SM. Interleukin-1 in the brain: mechanisms of action in acute neurodegeneration. Annals of the New York Academy of Sciences. 2003; 992:39–47. [PubMed: 12794045]

Pierre WC, Smith PL, Londono I, Chemtob S, Mallard C, Lodygensky GA. Neonatal microglia: The cornerstone of brain fate. Brain, behavior, and immunity. 2016

Pierre WC, Smith PL, Londono I, Chemtob S, Mallard C, Lodygensky GA. Neonatal microglia: The cornerstone of brain fate. Brain, behavior, and immunity. 2017; 59:333–345.

Prinz M, Priller J. Microglia and brain macrophages in the molecular age: from origin to neuropsychiatric disease. Nature reviews. 2014; 15:300–312.

Rolls A, Shechter R, London A, Ziv Y, Ronen A, Levy R, Schwartz M. Toll-like receptors modulate adult hippocampal neurogenesis. Nat Cell Biol. 2007; 9:1081–1088. [PubMed: 17704767]

Saito S, Matsuura M, Tominaga K, Kirikae T, Nakano M. Important role of membrane-associated CD14 in the induction of IFN-beta and subsequent nitric oxide production by murine macrophages in response to bacterial lipopolysaccharide. Eur J Biochem. 2000; 267:37–45. [PubMed: 10601848]

Savard A, Brochu ME, Chevin M, Guiraut C, Grbic D, Sebire G. Neuronal self-injury mediated by IL-1beta and MMP-9 in a cerebral palsy model of severe neonatal encephalopathy induced by immune activation plus hypoxia-ischemia. Journal of neuroinflammation. 2015; 12:111. [PubMed: 26025257]

Stridh L, Smith PL, Naylor AS, Wang X, Mallard C. Regulation of toll-like receptor 1 and -2 in neonatal mice brains after hypoxia-ischemia. Journal of neuroinflammation. 2011; 8:45. [PubMed: 21569241]

Strunk T, Inder T, Wang X, Burgner D, Mallard C, Levy O. Infection-induced inflammation and cerebral injury in preterm infants. The Lancet Infectious diseases. 2014; 14:751–762. [PubMed: 24877996]

Triantafilou M, Triantafilou K. Lipopolysaccharide recognition: CD14, TLRs and the LPS-activation cluster. Trends in immunology. 2002; 23:301–304. [PubMed: 12072369]

Turrin NP, Gayle D, Ilyin SE, Flynn MC, Langhans W, Schwartz GJ, Plata-Salaman CR. Pro-inflammatory and anti-inflammatory cytokine mRNA induction in the periphery and brain following intraperitoneal administration of bacterial lipopolysaccharide. Brain Res Bull. 2001; 54:443–453. [PubMed: 11306198]

Vallieres L, Rivest S. Regulation of the genes encoding interleukin-6, its receptor, and gp130 in the rat brain in response to the immune activator lipopolysaccharide and the proinflammatory cytokine interleukin-1beta. Journal of neurochemistry. 1997; 69:1668–1683. [PubMed: 9326296]

Visintin A, Mazzoni A, Spitzer JH, Wyllie DH, Dower SK, Segal DM. Regulation of Toll-like receptors in human monocytes and dendritic cells. J Immunol. 2001; 166:249–255. [PubMed: 11123299]

Wang KC, Wang SJ, Fan LW, Cai Z, Rhodes PG, Tien LT. Interleukin-1 receptor antagonist ameliorates neonatal lipopolysaccharide-induced long-lasting hyperalgesia in the adult rats. Toxicology. 2011; 279:123–129. [PubMed: 20937348]

Woo MS, Wang X, Faustino JV, Derugin N, Wendland MF, Zhou P, Iadecola C, Vexler ZS. Genetic deletion of CD36 enhances injury after acute neonatal stroke. Annals of neurology. 2012; 72:961–970. [PubMed: 23280844]

Yoon HJ, Jeon SB, Kim IH, Park EJ. Regulation of TLR2 expression by prostaglandins in brain glia. J Immunol. 2008; 180:8400–8409. [PubMed: 18523308]

Yuan TM, Sun Y, Zhan CY, Yu HM. Intrauterine infection/inflammation and perinatal brain damage: role of glial cells and Toll-like receptor signaling. Journal of neuroimmunology. 2010; 229:16–25. [PubMed: 20826013]

Ziegler G, Harhausen D, Schepers C, Hoffmann O, Rohr C, Prinz V, Konig J, Lehrach H, Nietfeld W, Trendelenburg G. TLR2 has a detrimental role in mouse transient focal cerebral ischemia. Biochemical and biophysical research communications. 2007; 359:574–579. [PubMed: 17548055]

Highlights

- TLR2 is highly expressed in early postnatal brain under physiological conditions
- Systemic LPS caused a robust induction of TLR2 in neonatal brain
- Acute sterile injury including stroke in neonates does not induce TLR2
- TLR2 response in neonates is mediated by resident microglia/macrophages

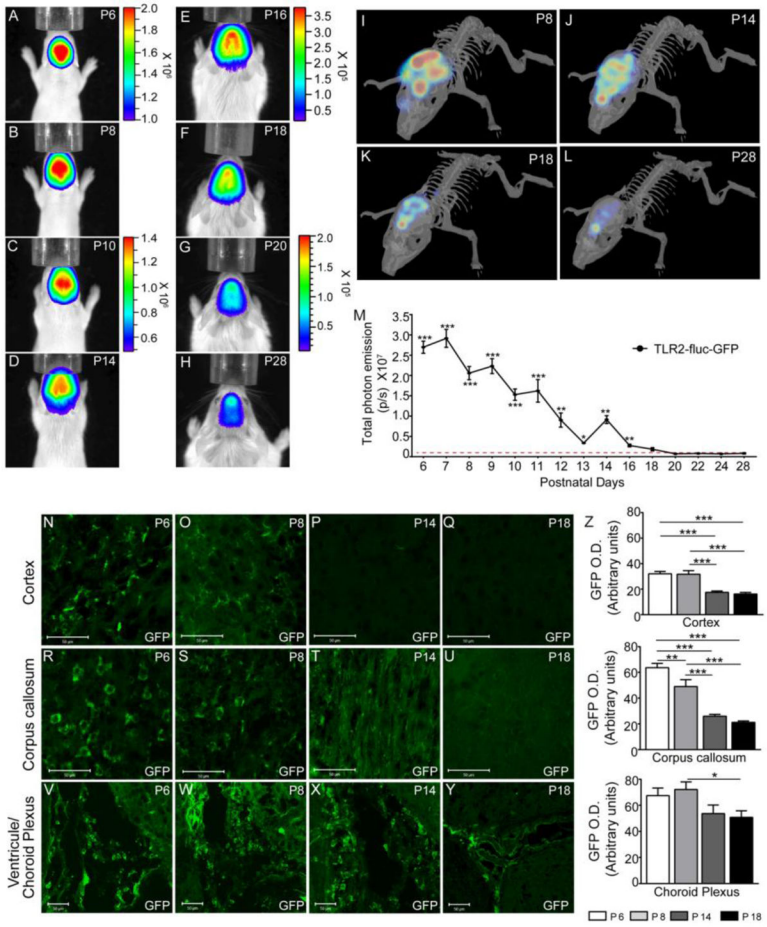

Figure 1. Real-time in vivo bioluminescent imaging of TLR2 expression in immature brain

(A–H) Representative images of bioluminescent signals in the brains of TLR2-luc-GFP mice during brain maturation between P6 and P28. Photographs of representative mice taken at different time points show that TLR2 expression decreases with brain maturation and becomes mostly restricted to the olfactory bulb by one month of age. The scales on the right are the color maps for source intensity. Note that the scale ranges differ at individual ages. (I–L) 3D reconstruction of bioluminescent signal at P8 (I), P14 (J), P18 (K) and P28 (L). (M) Quantification of the data obtained by measuring photon emission signal coming from the brain of the pups during the first month of life (in photons per second, p/s). (N–Y) Localisation of the GFP^+ signal by immunofluorescence in TLR2-luc-GFP mice confirmed the *in vivo* bioluminescent imaging data. GFP^+ cells show microglial morphology at P6 and P8 (N–O). Round shaped GFP^+ cells are observed at the same time point in the corpus callosum (R–S) and in the choroid plexus (V–W). At P14 and P18, very few GFP^+ cells are observed in the cortex (P–Q). Morphology of GFP^+ cells in the corpus callosum also changes with time to acquire an elongated shape at P14 (T) and star-like microglial shape at P18 (U). At both time points, GFP^+ cells are observed in the choroid plexus (X–Y). (Z) Quantification of GFP expression (optical density, arbitrary units) shows an overall decrease of GFP signal with time in the 3 regions analyzed. Note that GFP signal is the highest in the corpus callosum. One way ANOVA ***$p \leq 0.001$ ** $p \leq 0.01$ and *$p \leq 0.05$. Scale bar 50μm

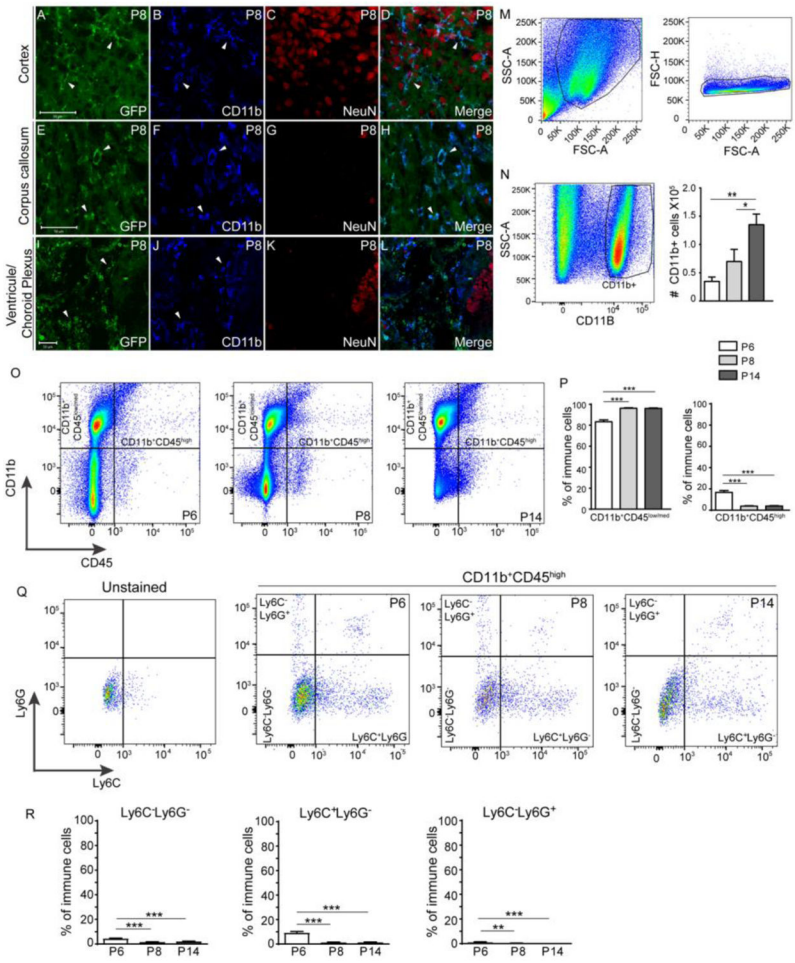

Figure 2. Identification of TLR2/GFP expressing cells in P8 mouse brain

(A–L) GFP expression is found in CD11b$^+$ microglial cells in P8 TLR2-luc-GFP mice. Double-immunofluorescence analysis using cell type specific markers in P8 brain reveals that GFP$^+$ cells are CD11b$^+$ but NeuN$^-$ in the cortex (A–D), in the corpus callosum (E–H) and in the choroid plexus (I–L). White arrowheads point to GFP$^+$CD11b$^+$ cells. (M) Gating strategy used in flow cytometry data analysis for choosing cells based on size (left panel) and single cells (right panel). **N**. Representative plots (left panel) and quantification (right panel) of CD11b$^+$ cell population in P6, P8, and P14 brain show significant increase of the total number of CD11b$^+$ cells during brain maturation. (O–P) Representative plots of CD11b and CD45 expression levels in P6, P8 and P14 brains (O). Quantification of CD11b$^+$CD45$^{low/med}$ population (top left quadrant in O) and CD11b$^+$CD45^{high} population (top right quadrant in O) demonstrates significantly higher % of CD11b$^+$CD45$^{low/med}$ in P8 and P14 brains (P, left panel), in parallel with significantly decreased CD11b$^+$CD45^{high} population in mice of same age (P, right panel). (Q–R) Identification of CD11b$^+$CD45^{high} cells (brain cells and/or monocytes and neutrophils infiltrated from the periphery) by Ly6C/Ly6G labeling at each time point. The plot of unstained cells was used to gate the Ly6C$^-$/Ly6G$^-$ population (Q). Quantification of plots in Q demonstrates the presence of 3 different populations, Ly6C$^-$/Ly6G$^-$ (R, left panel), Ly6C$^+$/Ly6G$^-$ (R, middle panel) and Ly6C$^-$/

Ly6G^{+} (R, right panel). Ly6C^{-}/Ly6G^{+} population constitutes less than 1% in all ages and significantly declines with age. A significant decrease in Ly6C^{+}/Ly6G^{-} population occurs from P6 to P14. One way ANOVA ***p≤0.001 ** p≤0.01 and *p≤0.05. Scale bar 50μm.

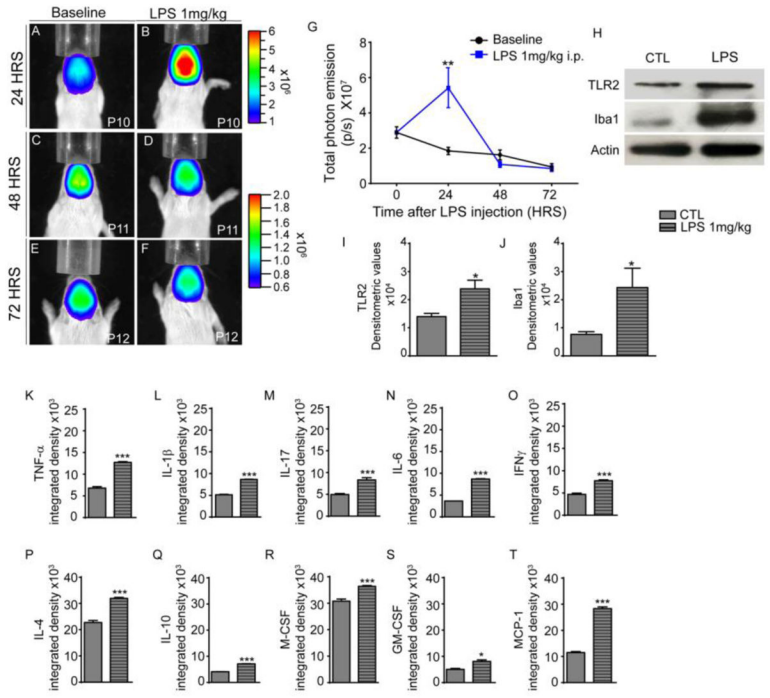

Figure 3. Inflammatory response in the immature brain after LPS injection

(A–F) Representative images of bioluminescent signals coming from the brains of TLR2-luc-GFP mice 24 to 72 hours after systemic (i.p.) LPS injection. A significant and transient increase in TLR2-luc signal (A–B) 24 hours after injection, with signal return to basal level by 48–72 hours. Scales on the right from images are color maps for signal intensity. Note scales are different at 24 and 48–72 hours. Plot of the data obtained by measuring photon emission in the brains after LPS injection (in photons per second, p/s) (G). (H–J) Representative western blot of TLR2 and Iba1 upregulation in brain homogenates 24 hours in CTL and LPS injected mice (H). Quantification of western blots revealed a significant increase of both TLR2 (I) and Iba1 (J) expression after LPS injection. (K–T) Protein expression of the 10 studied pro-inflammatory cytokines is rapidly increased following LPS injection as compared to saline injected mice. In fact, TNF-α (K), IL-1β (L), IL-17 (M), IL-6 (N), INF-γ (O) and MCP-1(T) are significantly increased. The levels of anti-inflammatory cytokines like IL-4 (P) and IL-10 (Q), as well as growth factors like M-CSF (R) and GM-CSF (S) also increase. Unpaired t-test ***p≤0.001 and *p≤0.05.

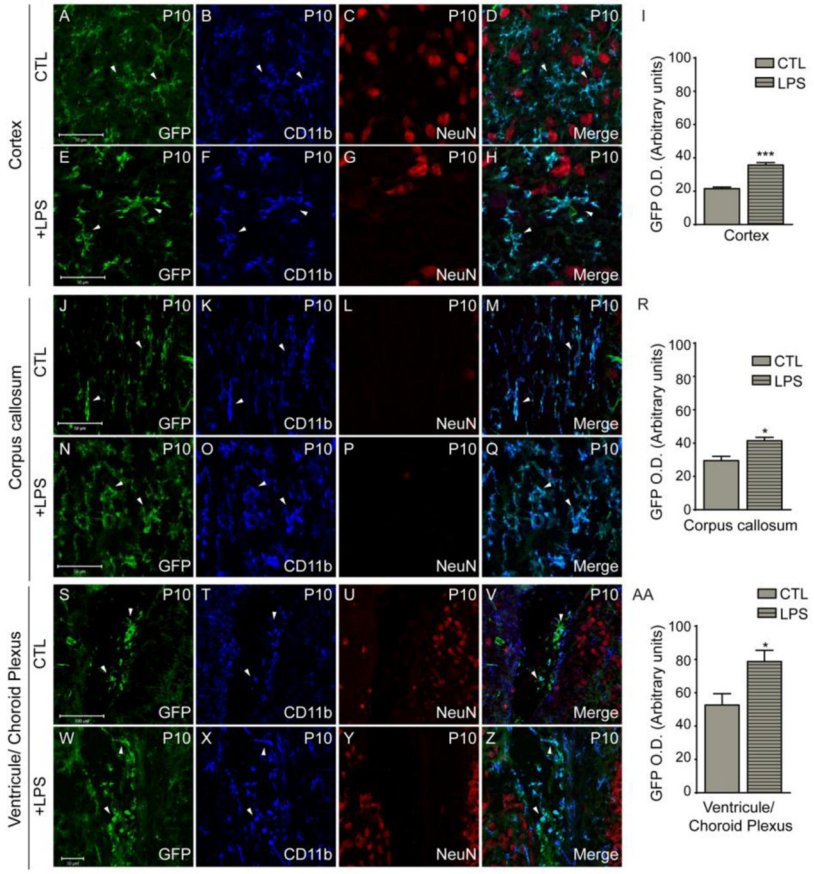

Figure 4. Identification of TLR2-GFP expressing cell types 24 hours after LPS injection

(A–Z) GFP is expressed in CD11b^{+} cells in multiple regions 24 hours after i.p. LPS injection in TLR2-luc-GFP P9 mice, including cortex (E–H), corpus callosum (N–Q) and the choroid plexus (W–Z). In LPS injected group, CD11b^{+} cells show a more activated morphology (E–H) compared to controls (CTL) (A–D). White arrowheads point to GFP $^{+}$CD11b^{+} cells. (I, R, AA) Quantification of GFP^{+} immunoreactivity (total OD signal per FOV) shows LPS-induced increase in GFP expression in the cortex (I), in the corpus callosum and the choroid plexus (AA). GFP $^{+}$ cells exhibit round and activated shape after LPS (N–Q) whereas microglial cells have elongated cell bodies and processes in CTL (J–M). Unpaired t-test ***p≤0.001 and *p≤0.05. Scale bar 50μm.

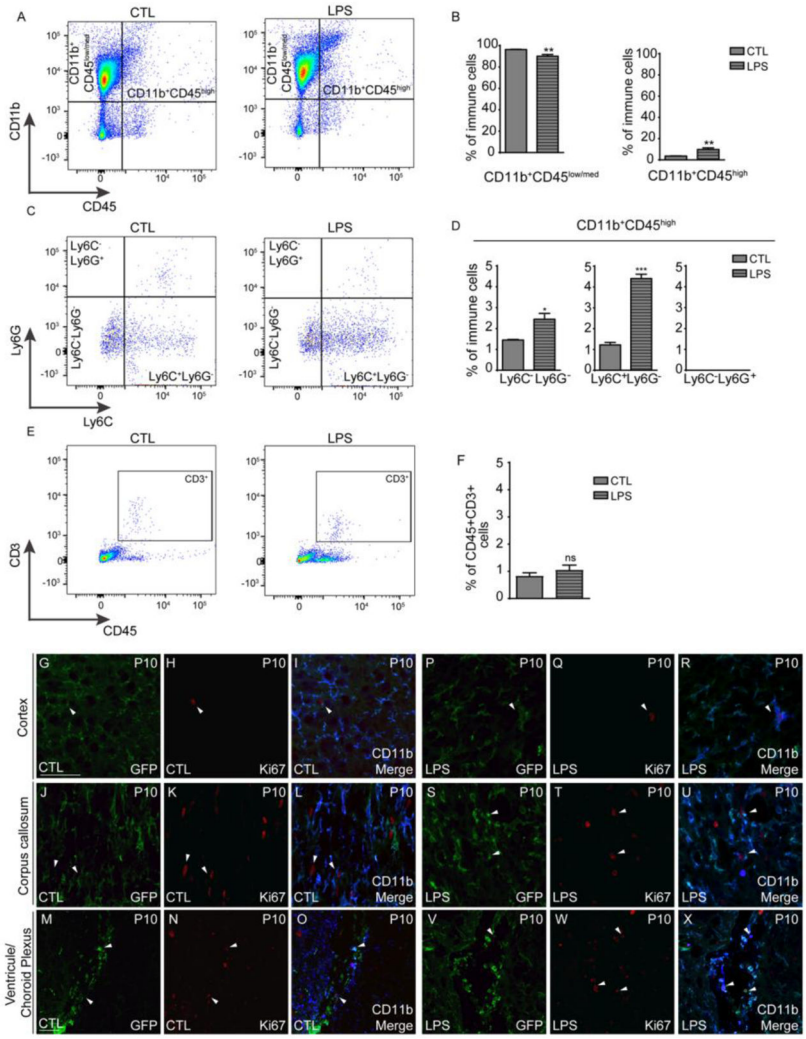

Figure 5. Increase in bioluminescent TLR2-luc signal is mostly triggered by microglial cells 24 hours after LPS injection

(A–B) Representative plots of gated cells selected by their expression level of $CD11b^{+}$ and $CD45^{+}$ in control mice (CTL) and in mice after LPS injected (A). Quantification of $CD11b^{+}CD45^{low/med}$ (top left quartile) and $CD11b^{+}CD45^{high}$ (top right quartile) populations revealed a small but significant decrease in the % of $CD11b^{+}CD45^{low/med}$ cells (B, left panel) in brains of LPS-treated mice. A significant increase was observed in $CD11b^{+}CD45^{high}$ population in LPS-treated mice (B, right panel). (C–D) The CD11b+CD45high population was further characterized by Ly6C/Ly6G staining (C). Quantification of the plots demonstrated the presence of three different populations, $Ly6C^{-}/Ly6G^{-}$ (D, left panel), $Ly6C^{+}/Ly6G^{-}$ (D, middle panel) and $Ly6C^{-}/Ly6G^{+}$ (R, right panel). Compared to CTR, LPS significantly increased % of $Ly6C^{-}/Ly6G^{-}$ and $Ly6C^{+}/Ly6G^{-}$ populations. The presence of $Ly6C^{-}/Ly6G^{+}$ neutrophils remained negligible in both groups. (E–F) Infiltration of $CD45^{+}/CD3^{+}$ lymphocytes was negligible in both CTL and LPS injected mice (G–X) Representative photomicrographs of GFP, CD11b and Ki67 expression in the cortex (G–I and P–R), corpus callosum (J–L and S–U) and choroid plexus (M–O and V–X) in CTL and

LPS injected mice. Ki67$^+$ proliferating GFP$^+$/CD11b$^+$ cells were seen in the cortex of both CTL and LPS injected mice. GFP$^+$/CD11b$^+$ microglial cells proliferate more in the corpus callosum and choroid plexus when compare to cortex (V–X). White arrowheads point to triple-positive GFP$^+$, CD11b$^+$ and Ki67$^+$ cells. One way ANOVA ***p≤0.001 ** p≤0.01 and *p≤0.05. Scale bar 50μm.

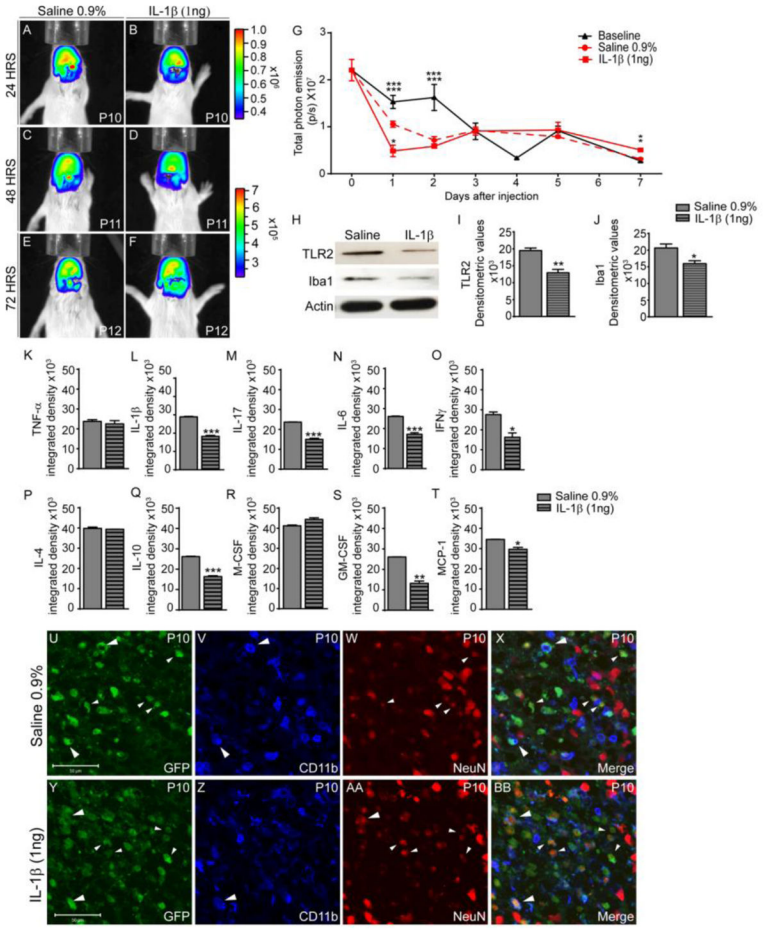

Figure 6. Intracortical IL-1β injection does induce TLR2-luc signal in neurons

(A–G) Representative images of bioluminescent signals in the brain of TLR2-luc-GFP P9 mice 24 to 72 hours following intra-cortical injection of IL-1β and saline 0.9% (A–F). Note the differing range of scales at individual time points (in photons per second, p/s). Compared to saline, injection of IL-1β leads to significant decrease in TLR2-luc signal within 24–72 hours (G). (H–J) Western blot analysis of TLR2 and Iba1 expression in brain homogenates 24 hrs after saline or IL-1β injection (H). Quantification of western blots revealed a significant decrease of both TLR2 (I) and Iba1 (J) expression after IL-1β injection when compared to saline. (K–T) At 24 hours after injection, the levels of several of the studied cytokines and chemokines are lower in brains of IL-1β injected mice than in saline-injected mice, including IL-17, IL-1β, IL-6, IFNγ, IL-10, GM-CSF and MCP-1. (U–BB) GFP^+ cells are $CD11b^+$ microglia and $NeuN^+$ neurons 24 hours after IL-1β injection. Around injection site, majority of the GFP^+ cells are $NeuN^+$ after saline (U–X) or IL-1β injection (Y–BB) 24 hours after injection. The shape of the microglial cells is different between the 2 groups. $CD11b^+$ cells are more round/amoeboid in saline treated mice (V) compared to a more star-like shaped cells in the IL-1β group (Z). White arrowheads point to GFP^+CD11b^+ cells. Small white arrowheads point to GFP^+NeuN^+ cells. One way ANOVA and Unpaired t-test ***p≤0.001, **p≤0.01 and *p≤0.05. Scale bar 50μm.

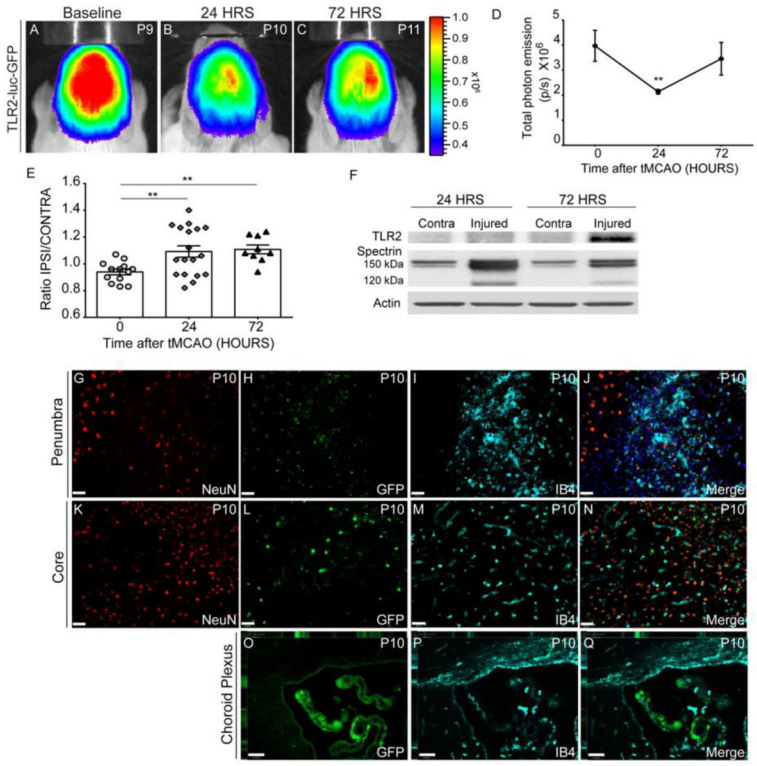

Figure 7. tMCAO in neonatal mice leads to a transient decrease in TLR2-luc signal

(A–E) Representative images of bioluminescent signal in the brain of TLR2-luc-GFP mice before and 24 to 72 hours after tMCAO produced in P9–P10 mice (A–C). The scales on the right are color maps for signal intensity. TLR2-luc signal is significantly and transiently decreased at 24 hours after tMCAO and is partially restored by 48 hours (B–C). Plot of the time course of photon emission signal (photons per second, p/s) (D). Changes of TLR2-luc photon emission signal in ipsilateral hemisphere compared to that in contralateral hemisphere in the same mice. Dots represent data from individual mice (E). (F) Representative western blot analysis of changes in TLR2 expression 24 and 72 hours after tMCAO. Spectrin cleavage (middle line) was used to confirm the presence of injury (150kDa band represents calpain-mediated spectrin cleavage. 120kDa band represents caspase-3 mediated spectrin cleavage). Note that injury is not associated with increased TLR2 expression at 24 hours but leads to increase in TLR2 expression at 72 hours. (G–Q) Immunofluorescence images show that GFP^+ cells are $IB4^+$ microglial cells in the penumbra (G–J) and in the ischemic core (K–N). Note that IB4 immunolabels microglial cells and vasculature and that GFP+ cells labels round $IB4^+$ cells. Also note that activated (round) $IB4^+$ cells clearly delineate the edge of the penumbra region. In the core, most of the GFP^+ cells are also $IB4^+$ with very few cell positive for NeuN. Some of the GFP^+ cells are negative for both markers. The majority of the GFP^+ cells located at the border of the ventricles are $IB4^+$ while in the choroid plexus, only a fraction of the GFP^+ cells are IB4 positives (O–Q). Scale bar 40 and 53μm

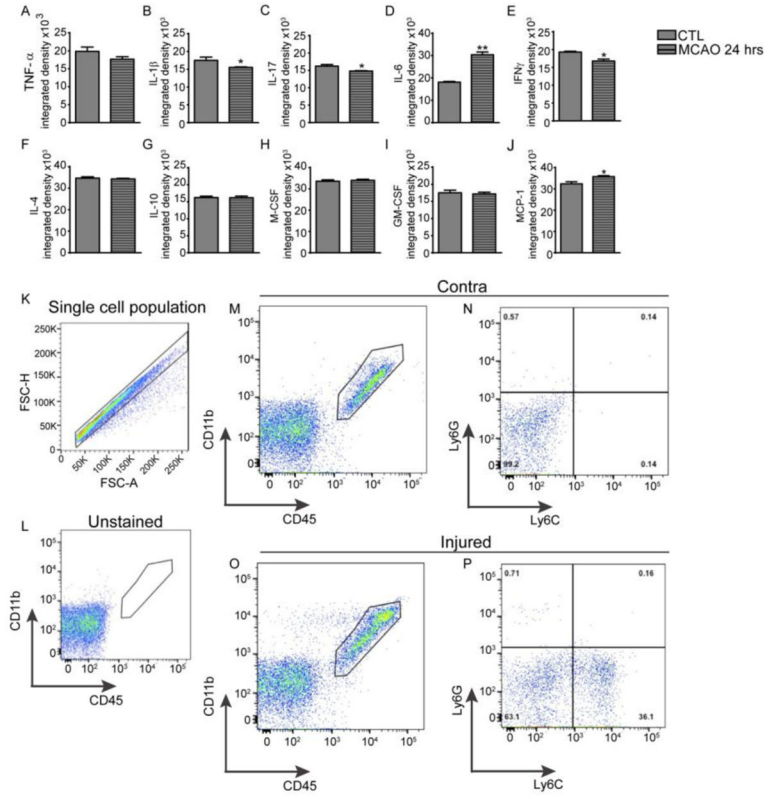

Figure 8. tMCAO activates cells of the monocyte lineage without producing major inflammatory response 24 hours after reperfusion

(A–J) The levels of inflammatory and anti-inflammatory cytokines and chemokines. Compared to the levels in contralateral hemisphere (Contra), there was significant increase in the levels of IL-6 and MCP-1 and a small but significant decrease in levels of IL-17, IL-1β and INFγ in injured regions (Injured). The levels of TNF-α, IL-10, IL-4, M-CSF and GM-CSF remained unchanged by injury. Unpaired t-test **p≤0.01 and *p≤0.05. (K–P) Representative examples of flow cytometry plots, including an example of gating strategy to choose single cells (K) and gating strategy (unstained sample, L). Representative plots of $CD11b^+/CD45^+$ cell populations in contralateral (M) and injured (N) regions. $CD11b^+/CD45^+$ gate was used to identify $Ly6C^+$ monocytes and $Ly6G^+$ neutrophils in contralateral (O) and injured (P) regions Note increased signal intensity of within the $CD45^+$ cell population in injured region (M–N), accumulation of $Ly6C^+$ monocytes but not Ly6G neutrophils in injured regions.<1% $Ly6G^+$ cells were seen in both contralateral and injured regions.